

Reaction of a Charge-Separated ONONO₂ Species with Water in the Formation of HONO: an MP2 Molecular Dynamics Study

Mychel E. Varner^{†}, Barbara J. Finlayson-Pitts[†] and R. Benny Gerber^{†‡}*

[†]Department of Chemistry, University of California, Irvine, CA 92697-2025. [‡]Institute of Chemistry and Fritz Haber Research Center for Molecular Dynamics, The Hebrew University of Jerusalem, Israel, 91904.

Supporting Information

Details of the Calculations

In the current work, structures were first optimized using the scaled opposite-spin second-order Moller-Plesset method with the resolution of identity approximation [SOS-RIMP2].^{1,2} The Karlsruhe SVP basis set was employed with added diffuse functions from the Dunning aug-cc-pVDZ basis set [aSVP].³⁻⁶ In test calculations, diffuse functions were necessary for correct energetic ordering of the isomers and the use of the SOS method improved the MP2 relative energies compared to coupled-cluster singles and doubles [CCSD] single point calculations.⁷ The clusters studied here were also optimized at the SOS-RIMP2/aug-cc-pVTZ and SOS-RIMP2/aug-cc-pVDZ levels and the energies were subsequently determined at the CCSD/aug-cc-pVTZ level [CCSD/aTZ//SOS-RIMP2/aTZ] and at the CCSD(T)/aug-cc-pVDZ level [CCSD(T)/aDZ//SOS-RIMP2/aDZ].^{1,2,4,6-9} Core electrons were excluded from all correlation calculations. In SOS-RIMP2/aSVP optimizations, energies were converged to 10⁻⁸ au and gradients to 10⁻⁷ au/bohr; harmonic frequency calculations indicated that all clusters are either minima with no imaginary frequencies or transition states with one imaginary frequency. With

the larger aDZ and aTZ basis sets, energies were converged to 10^{-6} au and gradients to 10^{-3} au/bohr.

The SOS-RIMP2/aSVP approach was used in MD simulations. Partial charges were determined using natural population analysis.¹⁰ Beginning from the TS, velocities were randomly assigned based on a temperature of either 50 K or 300K and trajectories were propagated at constant energy with a time step of 20 au. Velocities at the starting configuration were then reversed and also propagated at constant energy. In dynamics simulations drift in the total energy was on the order of 10^{-5} au/ps or less. All calculations were performed with the TURBOMOLE program package.¹¹

Relative Energies at Additional Levels of Theory

In summarizing previous work and introducing the methods used in this work, it was mentioned that the description of the $\text{ONONO}_2 \rightarrow (\text{NO}^+)(\text{NO}_3^-) \rightarrow \text{TS}$ reaction energies were qualitatively incorrect at the B3LYP level, with an insufficient basis and with MP2 without spin component scaling. In the test calculations demonstrating this, two additional structures were included: (i) the sym- $\text{N}_2\text{O}_4 \cdot (\text{H}_2\text{O})_4$ cluster with a square water configuration and (ii) the previously mentioned $(\text{NO}^+)(\text{NO}_3^-) \cdot (\text{H}_2\text{O})_4$ cluster with a branched water configuration. The B3LYP/6-311++G(3df,3pd), RIMP2/SVP, RIMP2/aSVP, SOS-RIMP2/aSVP and CCSD/aTZ relative energies (at the SOS-RIMP2/aTZ geometry) of these additional structures and those from Figure 1 are presented in Table S1. As the focus of this work was on the role of the charge-separated species in the proton transfer process, the SOS-RIMP2/aSVP level of theory, which correctly describes the *trans*- $\text{ONONO}_2 \cdot (\text{H}_2\text{O})_4$ branched, $(\text{NO}^+)(\text{NO}_3^-) \cdot (\text{H}_2\text{O})_4$ branched and the TS clusters, was employed in the simulations.

Table S1. Relative energies of reactant, transition state (TS) and product clusters at various levels of theory.

Cluster	B3LYP Pople TZ ^a (kcal/mol) ^b	RIMP2 SVP (kcal/mol) ^b	RIMP2 aSVP (kcal/mol) ^b	SOS-RIMP2 aSVP (kcal/mol) ^b	CCSD aTZ (kcal/mol) ^b
i) sym-N ₂ O ₄ •(H ₂ O) ₄ square	-11	-21	-19	-14	-3
a) <i>trans</i> -ONONO ₂ •(H ₂ O) ₄ square	0	0	0	0	0
b) <i>trans</i> -ONONO ₂ •(H ₂ O) ₄ branched	3	5	3	3	3
ii) (NO ⁺)(NO ₃ ⁻)•(H ₂ O) ₄ branched	2	0	2	5	5
c) TS: proton transfer to NO ₃ ⁻	4	2	5	7	6
d) TS: proton transfer to H ₂ O	3	-1	3	7	6
e) <i>cis</i> -HONO•HONO ₂ •(H ₂ O) ₂	-3	-3	2	0	-5
f) <i>trans</i> -HONO•(NO ₃ ⁻)•(H ₃ O ⁺)•(H ₂ O) ₂	-5	-7	0	3	-3

^a6-311++G(3df,3pd) ^bAt the SOS-RIMP2/aTZ geometry.

As mentioned in the discussion of the results presented in Table 1, the predicted stability of the product clusters relative to the *trans*-ONONO₂•(H₂O)₄ minimum is more sensitive to the basis size and method. To demonstrate the variation in relative energies with basis size and method for higher levels of theory, the CCSD/aug-cc-pVDZ and CCSD(T)/aug-cc-pVTZ energies, determined at the SOS-RIMP2/aug-cc-pVDZ structure, and CCSD/aug-cc-pVTZ energies, determined at the SOS-RIMP2/aug-cc-pVTZ structure, are included in Table S2. Reaction energies for the *trans*-ONONO₂•(H₂O)₂ cluster including the CCSD(T)/aug-cc-pVTZ energy are presented in Table S3.

The aDZ-aTZ basis effect is ~2 kcal/mol with the product stability increasing with the increased basis size. However, the CCSD(T) calculations indicate that product stability is overestimated at the CCSD level. The perturbative triples correction is about 3 kcal/mol for the neutral product cluster relative to the *trans*-ONONO₂•(H₂O)₄ minimum. Additional refinement of the product stability would be of interest, but is not crucial to this work as the lower level of theory gives a qualitatively good description of the reactant and transition state energetics and formation of the products from the transition states is sufficiently exothermic to prevent the reverse reaction in the short simulations presented here.

Table S2. Relative energies of reactant, transition state (TS) and product clusters comparing the basis size effect and perturbative triples correction.

Cluster	CCSD aDZ (kcal/mol) ^a	CCSD aTZ (kcal/mol) ^b	CCSD(T) aDZ (kcal/mol) ^a
a) <i>trans</i> -ONONO ₂ •(H ₂ O) ₄ minimum	0.0	0.0	0.0
b) <i>trans</i> -ONONO ₂ •(H ₂ O) ₄ branched	2.8	3.3	3.4
c) TS: proton transfer to NO ₃ ⁻	6.5	5.8	6.3
d) TS: proton transfer to H ₂ O	6.3	5.7	5.2
e) <i>cis</i> -HONO•HONO ₂ •(H ₂ O) ₃	-3.3	-4.9	-0.1
f) <i>trans</i> -HONO•(NO ₃ ⁻)•(H ₃ O ⁺)•(H ₂ O) ₂	-1.3	-3.2	-0.2

^aAt SOS-RIMP2/aDZ geometry. ^bAt SOS-RIMP2/aTZ geometry.

Table S3. Relative energies of reactant, transition state (TS) and product clusters with one reacting H₂O and one solvating H₂O comparing the basis size effect and perturbative triples correction.

Cluster	CCSD aDZ ^a (kcal/mol)	CCSD aTZ ^b (kcal/mol)	CCSD(T) aDZ ^a (kcal/mol)	CCSD(T) aTZ ^b (kcal/mol)
a) <i>trans</i> -ONONO ₂ •(H ₂ O) ₂	0.0	0.0	0.0	0.0
b) TS: proton transfer to NO ₃ ⁻	9.5	9.3	9.0	8.9
c) HONO ₂ • <i>cis</i> -HONO•H ₂ O	-6.0	-8.4	-2.6	-5.2

^aAt SOS-RIMP2/aDZ geometry. ^bAt SOS-RIMP2/aTZ geometry.

The *cis*-ONONO₂•(H₂O)₄ Isomer

Though the current work focused on the reaction of the *trans*-ONONO₂ isomer, a transition state for the reaction within a *cis*-ONONO₂•(H₂O)₄ cluster to form HONO was also identified. This transition state is 3.5 kcal/mol above the transition states presented in Figure 1 and 8.3 kcal/mol above the *cis*-ONONO₂•(H₂O)₄ cluster with a branched water configuration. These *cis*-ONONO₂•(H₂O)₄ structures are presented in Figure S1. The *cis*-ONON configuration does not allow the reacting water to easily insert between the NO and NO₃ fragments. In the transition state structure from the *trans*-ONONO₂ isomer, the insertion of the reacting water between the counterions shields the charges and forms a stabilizing hydrogen bond with the NO₃⁻ anion. Additional solvation may lower the reaction barrier, however if the barrier for reaction of *cis*-ONONO₂ with H₂O at a water surface remains higher than those for *cis-trans* isomerization and the reaction of the *trans* isomer, reaction of the *trans* isomer would be preferred.

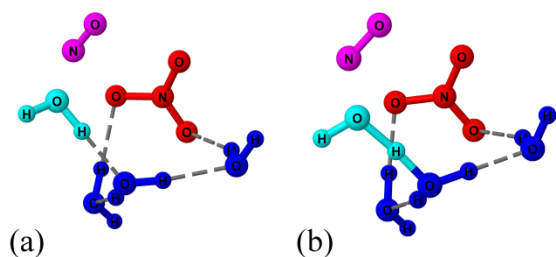


Figure S1. Structures of (a) *cis*-ONONO₂•(H₂O)₄ branched cluster [ON-ONO₂ distance = 1.98 Å; H₂O-NO distance = 2.56 Å] and (b) the TS for proton transfer to H₂O [ON-ONO₂ distance = 2.49 Å; H₂O-NO distance = 1.90 Å]. The NO₃ fragment is red, NO fragment is magenta; H₂O is blue with the reacting H₂O a lighter blue.

Additional Trajectories

The six additional trajectories for each of the simulations presented in the main text are included here. The seven trajectories for proton transfer to the NO_3^- anion are overlaid in Figure S3. One trajectory deviates from the behavior described in the main text by forming the product cluster in both the forward and reverse trajectories. The same is true for the simulation of proton transfer to the neighboring water in Figure S4. In these additional trajectories, there is greater variation in the time at which the charge separation reaches that of the reactant cluster, $\delta(\text{NO}^+) - \delta(\text{NO}_3^-)$, but the magnitude of the maximum charge separation is quite consistent, roughly 1.5 to 1.6. Three of the additional trajectories for proton transfer to the water with greater total energy (Figure S5) deviate from the behavior shown in the main text. In these three trajectories, the reactant cluster was formed at both positive and negative times. Again, these additional trajectories show some variation in the time to pass through the region of greater charge separation, but consistency in the magnitude of the maximum charge separation. One of the additional trajectories that forms the initial *trans*- $\text{HONO} \cdot (\text{NO}_3^-) \cdot (\text{H}_3\text{O}^+) \cdot (\text{H}_2\text{O})_2$ product cluster, goes on to form the *trans*- $\text{HONO} \cdot \text{HONO}_2 \cdot (\text{H}_2\text{O})_3$ product cluster through proton transfer along a water wire as indicated by a significant drop in the charge separation at roughly 0.75 ps.

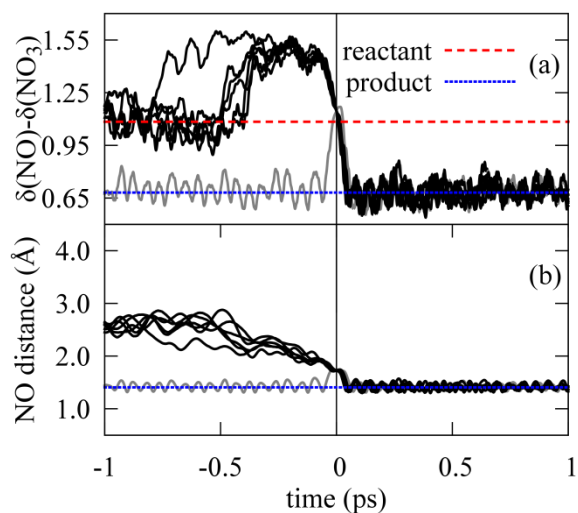


Figure S2. Plots of (a) the difference in the partial charges on the NO and NO₃ fragments, $\delta(\text{NO}) - \delta(\text{NO}_3)$, and (b) the HO-NO distance versus time for a low energy simulation demonstrating the formation of *cis*-HONO and HONO₂ from *trans*-ONONO₂ and H₂O. Reference values are indicated by dashed horizontal lines for the *trans*-ONONO₂•(H₂O)₄ branched reactant cluster (red) and *cis*-HONO•HONO₂•(H₂O)₃ product cluster (blue). Seven trajectories are overlaid, with one forming the product cluster when velocities are propagated both to positive and negative time (grey).

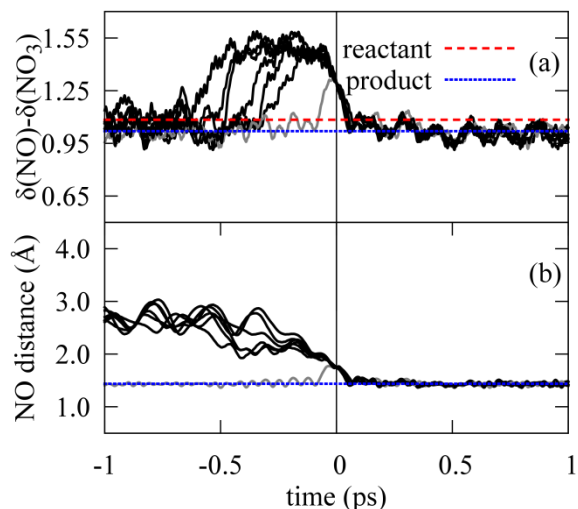


Figure S3. Plots of (a) the difference in the partial charges on the NO and NO₃ fragments, $\delta(\text{NO}) - \delta(\text{NO}_3)$, and (b) the HO-NO distance versus time for a low energy simulation demonstrating the formation of *trans*-HONO, NO₃⁻ and H₃O⁺ from *trans*-ONONO₂ and H₂O. Reference values are indicated by dashed horizontal lines for the *trans*-ONONO₂•(H₂O)₄ branched reactant cluster (red) and the *trans*-HONO•(NO₃⁻)•(H₃O⁺)•(H₂O)₂ product cluster (blue). Seven trajectories are overlaid, with one forming the product cluster when velocities are propagated both to positive and negative time (grey).

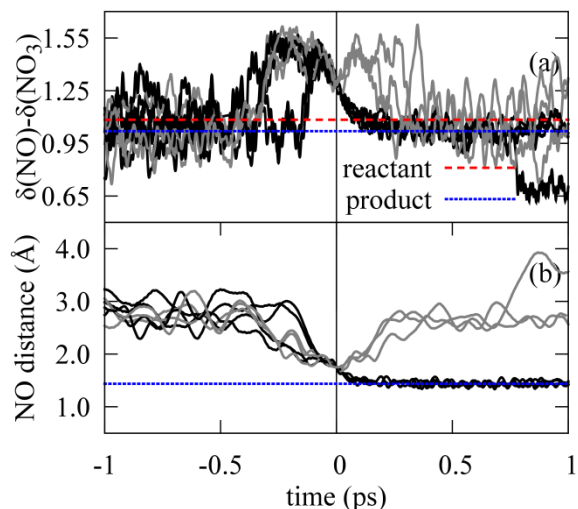


Figure S4. Plots of (a) the difference in the partial charges on the NO and NO₃ fragments, $\delta(\text{NO}) - \delta(\text{NO}_3)$, and (b) the HO-NO distance versus time for a high energy simulation demonstrating the formation of *trans*-HONO and HONO₂ from *trans*-ONONO₂ and H₂O. Reference values are indicated by dashed horizontal lines for the *trans*-ONONO₂•(H₂O)₄ branched reactant cluster (red) and the *trans*-HONO•(NO₃⁻)•(H₃O⁺)•(H₂O)₂ product cluster (blue). Seven trajectories are overlaid, with three forming the reactant cluster when velocities are propagated to positive and negative time (grey).

1. F. Weigend and M. Häser, *Theor Chem Acta*, 1997, **97**, 331–340.
2. Y. Jung, R. C. Lochan, A. D. Dutoi, and M. Head-Gordon, *The Journal of Chemical Physics*, 2004, **121**, 9793–9802.
3. A. Schäfer, H. Horn, and R. Ahlrichs, *The Journal of Chemical Physics*, 1992, **97**, 2571–2577.
4. R. A. Kendall, T. H. Dunning, and R. J. Harrison, *The Journal of Chemical Physics*, 1992, **96**, 6796–6806.
5. F. Weigend, M. Häser, H. Patzelt, and R. Ahlrichs, *Chemical Physics Letters*, 1998, **294**, 143–152.
6. F. Weigend, A. Köhn, and C. Hättig, *The Journal of Chemical Physics*, 2002, **116**, 3175–3183.
7. G. D. Purvis and R. J. Bartlett, *The Journal of Chemical Physics*, 1982, **76**, 1910–1918.
8. T. H. Dunning, *The Journal of Chemical Physics*, 1989, **90**, 1007–1023.
9. K. Raghavachari, G. W. Trucks, J. A. Pople, and M. Head-Gordon, *Chemical Physics Letters*, 1989, **157**, 479–483.
10. A. E. Reed, R. B. Weinstock, and F. Weinhold, *The Journal of Chemical Physics*, 1985, **83**, 735–746.
11. TURBOMOLE V6.3 2011, a development of University of Karlsruhe and Forschungszentrum Karlsruhe GmbH, 1989-2007, TURBOMOLE GmbH, since 2007; available from <http://www.turbomole.com>, .